NANO LETTERS

pubs.acs.org/NanoLett Letter

Improved Carrier Lifetime in $BiVO_4$ by Spin Protection

Chunyang Zhang,[▽] Yongliang Shi,[▽] Yitao Si,[▽] Maochang Liu,* Liejin Guo, Jin Zhao, and Oleg V. Prezhdo*

Cite This: *Nano Lett.* 2022, 22, 6334−6341 Read Online

ACCESS | Metrics & More | Article Recommendations | Supporting Information

ABSTRACT: Mechanistic understanding of the effect bulk defects have on carrier dynamics at the quantum level is crucial to suppress associated midgap mediated charge recombination in semiconductors yet many questions remain unexplored. Here, by employing ab initio quantum dynamics simulation and taking $BiVO_4$ with oxygen vacancies (Ov) as a model system we demonstrate a spin protection mechanism for suppressed charge recombination. The carrier lifetime is significantly improved in the high spin defect system. The lifetime can be optimized by tuning the Ov concentration to minimize the nonradiative relaxation. Our work addresses literature ambiguities and contradictions about the role of bulk Ov in charge recombination and provides a route for defect engineering of semiconductors with enhanced carrier dynamics.

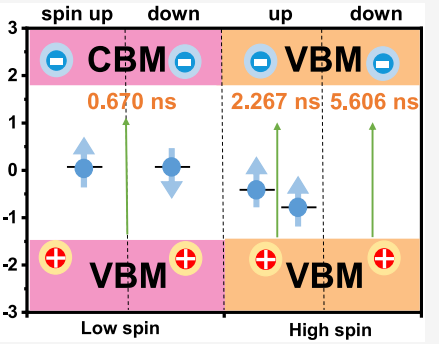

KEYWORDS: *Carrier lifetime, spin protection, oxygen vacancy, bismuth vanadate, ab initio quantum dynamics, nonadiabatic coupling*

Carrier dynamics in semiconductors is central to many solar energy conversion and optoelectronic technologies and devices.[1−12] Photoinduced charges generally should have relatively long lifetimes, which demands perfect materials.[13,14] However, in practice thermodynamically stable defects are prevalent in semiconductors and are hard to remove.[15,16] Such defects, especially in semiconductor bulk, introduce midgap energy levels that mediate charge recombination and are very effective lifetime killers.[17,18] Therefore, semiconductor defects need to be carefully designed and controlled to achieve desired carrier dynamics performance by suppressing charge recombination.

Figure 1a summarizes the three common types of point defects in semiconductors: interstitial defects, substitutional defects, and vacancy defects. The presence of defects often produces trap states in the band gap. According to the Shockley−Read−Hall (SRH)[19] recombination model, photogenerated electron and hole pairs (e-h) can recombine more quickly via pathways 1 and 2 (by-defect recombination, conduction band maximum (CBM)-trap-valence band maximum (VBM)) than pathway 3 (direct recombination, CBM-VBM) (Figure 1b). As a result, a significant amount of photon energy is converted into heat via rapid nonradiative recombination, which greatly reduces the solar energy conversion and optoelectronic efficiencies. Thus, Yang et al.[20] demonstrated that the number of defects should be minimized in order to avert the formation of SRH recombination centers. The authors doubled the device performance by reducing the concentration of oxygen vacancies (Ov) in $BiVO_4$. However, other works demonstrate that the introduction of abundant vacancy defects into semiconductors yield improved carrier dynamics.[21−25] Wang et al.[26] adjusted the concentration of Ov in $BiVO_4$ and found that the carrier lifetime in the $BiVO_4$ system with a relatively higher content of Ov was almost twice as long as that with a relatively lower content which is a direct contradiction to the SRH model. They suggested that Ov provide photoinduced charge traps that promote charge separation and extend carrier lifetime. This apparent contradiction regarding the influence of defect density on the carrier lifetime may arise in part because defect-induced spontaneous spin symmetry breaking of the electronic structure is not considered. Few papers have studied spin polarization of these materials, as most semiconductor defects are traditionally considered spin symmetric. Pan et al.[24] enhanced the carrier lifetime in anatase TiO_2 by regulating the density of Ti vacancies. Notably, the introduction of Ti vacancies into anatase caused room-temperature paramagnetism, and the carrier lifetime was proportional to the intensity of spin polarization. The authors suggested that electrons may lose the original spin direction during the electron transfer and inhibit the recombination.[24] Motivated by the conflicting experimental evidence regarding the influence of Ov concentration on the charge carrier lifetimes in $BiVO_4$ and the experimental indication that spin polarization can have a

Received: May 23, 2022
Revised: July 23, 2022
Published: July 27, 2022

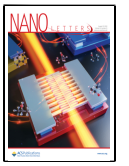

https://doi.org/10.1021/acs.nanolett.2c02070
Nano Lett. 2022, 22, 6334−6341

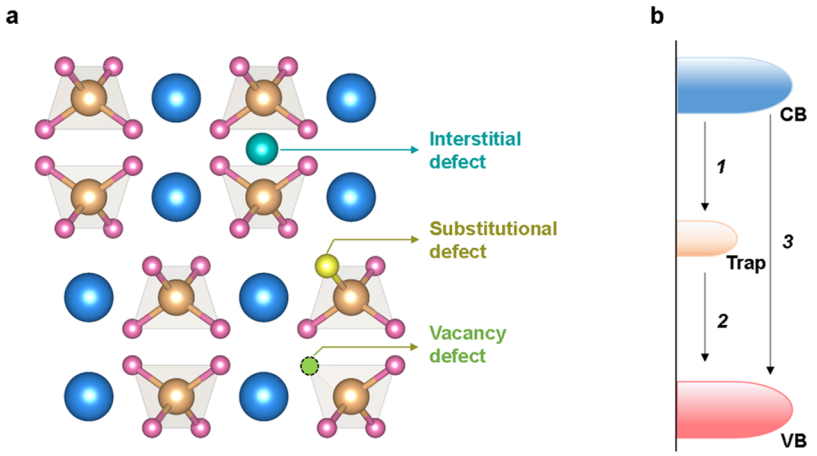

Figure 1. Model of the defect-induced e-h recombination center via the Shockley–Read–Hall (SRH) process. (a) Three common defects are the following: the interstitial defect is depicted in navy blue, the substitutional defect in yellow, and the vacancy defect in green. (b) Schematic of fast e-h recombination via the SRH process. There are two pathways for the e-h recombination in the defective systems, and the by-defect recombination (paths 1 and 2) dominates over the direct recombination (path 3).

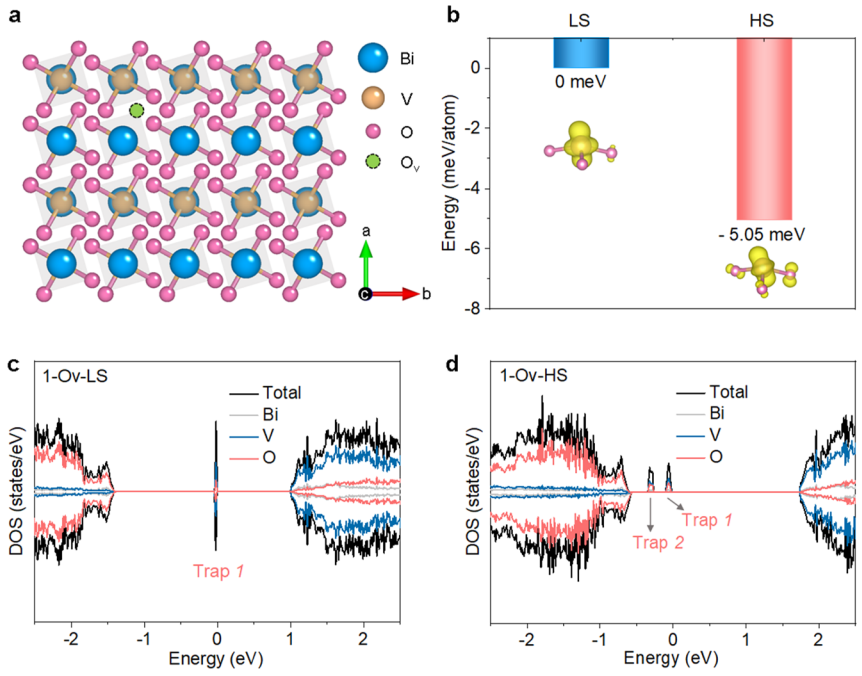

Figure 2. Ground state information on the 1-Ov $BiVO_4$ systems with different spin states. The defect states are all filled with electrons in both the 1-Ov-LS and 1-Ov-HS systems, hence they act as hole traps. (a) Atomic structure of the 1-Ov system. Green spheres indicate the defect location. (b) Energy per atom of 1-Ov-LS (left) and 1-Ov-HS (right). The energy reference is the 1-Ov-LS system. The difference between the energies of the simulation cell in the low and high spin states is 479.75 meV. The insets show orbital spatial distribution of Trap 1 for the two 1-Ov systems. (c) Density of states for 1-Ov-LS. The trap states (Trap 1) are located in the middle of the gap. (d) Density of states for 1-Ov-HS. The trap states (Trap 1 and Trap 2) are located near the VBM. The Fermi energy is set to 0.

significant influence on the carrier lifetime in defective TiO_2, we set out to consider explicitly spin polarization in the study of carrier dynamics of defective semiconductors, focusing on Ov in $BiVO_4$. The common presence of Ov in metal-oxide semiconductors makes them particularly pertinent for investigation as a general model.

In this work, using $BiVO_4$ with varying numbers of oxygen vacancies as a model system and studying it using time-domain ab initio nonadiabatic molecular dynamics, we demonstrate for the first time a spin protection mechanism (SPM) based upon enhanced spin polarization of defects to improve significantly the carrier lifetime in $BiVO_4$. Enhancing spin polarization not only transfers all the trap states to one spin channel but also moves the trap states from the intermediate position to near the valence band with both factors improving the carrier lifetime. In addition, we find that competition between the atom thermal motion-assisted electron–phonon coupling and the overlap of the electron and hole states can be mediated by adjusting the Ov concentration to maximize the SPM effect.

We first investigated two spin polarizations for 1-Ov (where x in x-Ov is the number of oxygen atoms removed from the pristine $BiVO_4$ supercell ($2 \times 2 \times 1$)) (Figure 2a) with symmetric low spin states (1-Ov-LS) and asymmetric high spin states (1-Ov-HS). Structure models were carried out using the

https://doi.org/10.1021/acs.nanolett.2c02070
Nano Lett. 2022, 22, 6334–6341

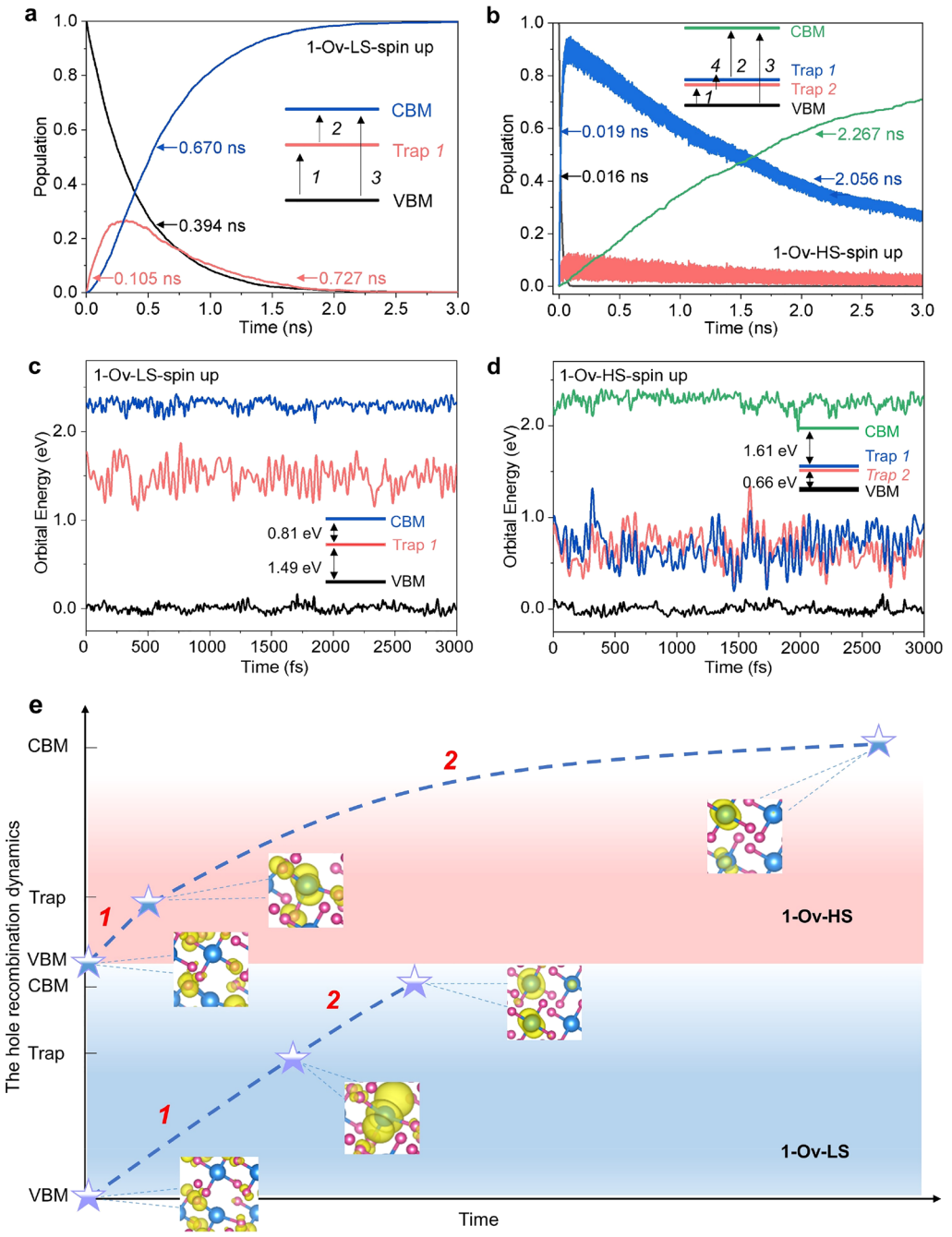

Figure 3. Hole trapping and recombination dynamics in the spin-up channel for (a) 1-Ov-LS and (b) 1-Ov-HS. The VBM population decreases due to hole trapping. Upon e-h recombination the hole reaches the CBM, and its population increases. Time evolution of the VBM, the CBM, and the defect states in the spin-up channel for (c) 1-Ov-LS and (d) 1-Ov-HS. The colors of the state populations and energies match the colors of the states on the diagrams in the insets. (e) Schematic of the e-h recombination process for the 1-Ov-LS and 1-Ov-HS systems.

Device Studio program.[27] Generally, the charge state of the oxygen vacancy depends on doping and applied fields. The systems under investigation are neutral, and oxygen vacancy levels are occupied. As shown in the histogram in Figure 2b, the relative energy of l-Ov-LS is higher than 1-Ov-HS, consistent with Hund's rule.[28] The energy difference between the low and high spin states is 479.75 eV per simulation cell with one vacancy. This is about 19 times larger than k_BT at room temperature, indicating that over 99% of the vacancies are in the high spin state in thermodynamic equilibrium. The high spin configuration can be stabilized further by application of an external magnetic field.[29] The relative stability of high and low spin states can be modified by introducing charges, dopants, strain, and so forth.

The density of states (DOS) of 1-Ov-LS (Figure 2c) and 1-Ov-HS (Figure 2d) shows that the main contributions to the VBM and the CBM are O 2p and V 3d orbitals, respectively, while the main contributions to the trap states are V 3d and O 2p. We define the defect state closest to the Fermi level as Trap 1. For 1-Ov-LS, the trap states are symmetric in the spin-up and down channels and are located in the middle of the band gap. These defect states can easily lead to the SRH recombination of e-h pairs. For 1-Ov-HS, however, the defect states are all in the spin-up channel and near the VBM.

https://doi.org/10.1021/acs.nanolett.2c02070
Nano Lett. 2022, 22, 6334−6341

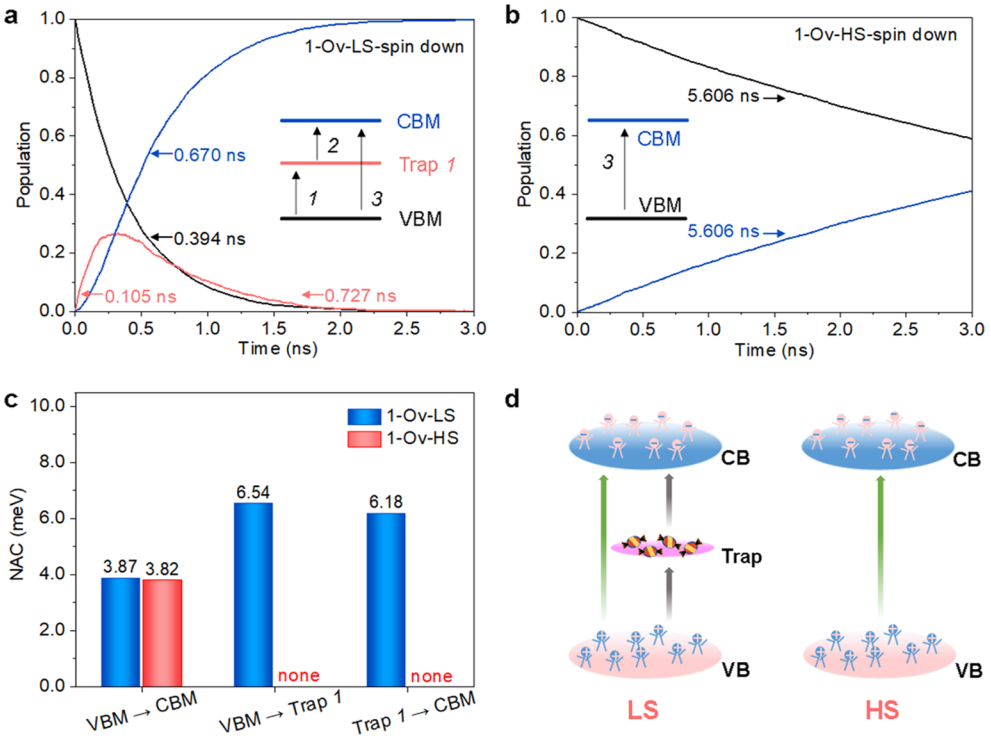

Figure 4. Hole trapping and recombination dynamics in the spin-down channel for (a) 1-Ov-LS and (b) 1-Ov-HS. The VBM population (black) decreases and the CBM population (blue) increase as the hole leaves the VBM and recombines with the electron in the CBM. (c) Root-mean-square of the NAC between the VBM, the CBM, and the defect states in the spin-up channel for 1-Ov-LS (blue) and 1-Ov-HS (red). (d) Schematic of the e-h recombination process for 1-Ov-LS (left) and 1-Ov-HS (right).

Because of the differing electronic structures of the two 1-Ov systems, it is reasonable to expect that the carrier recombination dynamics also are different. For clarity, we describe the carrier dynamics of the spin-up channel and spin-down channel of the two systems in turn. An oxygen vacancy gives off two surplus electrons to the defect states, the defect states are all filled with electrons in both 1-Ov-LS and 1-Ov-HS systems. Because the defect levels are filled, the photoexcited electrons in CBM cannot directly relax to the trap level. Hence, the carrier dynamics discussed in this report are hole dynamics. Here, for the direct recombination the holes in the VBM recombine with electrons in the CBM. By-defect recombination is a two-step process where, first, the holes relax from the VBM to the trap states. Then, the holes of the trap states recombine with electrons of the CBM, and the electronic system returns to the ground state.

Figure 3 shows the hole trapping and recombination dynamics information for 1-Ov-LS and 1-Ov-HS in the spin-up channel (see Figures S1 and S2 for more information). The insets in Figure 3a,b show the hole−electron recombination pathways. The difference between the two systems is that for 1-Ov-HS there is an additional trap in-band transition (Trap 2 to Trap 1, path 4). The time of transition 4 is 0.189 ps which is much faster compared with the other transitions due to the small energy difference between the initial and final states (Figure S2b). For 1-Ov-LS and 1-Ov-HS, the transition times for path 1 are 0.425 ns and 16.498 ps, respectively, and for path 2 the transition times are 0.255 and 2.042 ns, respectively (Table S1). In other words, for 1-Ov-HS the recombination rate of path 1 is faster and of path 2 slower than 1-Ov-LS. The result is that the e-h recombination in 1-Ov-LS is faster than in 1-Ov-HS by a factor of 3.4 (0.670 and 2.267 ns, respectively). This can be explained by the nonadiabatic coupling (NAC) matrix (Figure S3a,b). NAC represents the inelastic electron-vibrational scattering that determines the carrier dynamics, and carrier lifetime decreases with increasing NAC.[30−32] According to eq S1, the NAC value is correlated inversely with the energy difference between the two states and is proportional to the atomic velocity and the electron−phonon interaction matrix element. More information on the factors influencing the NAC is also shown in Figures S4−S6. In our case, the nuclear velocity[33] and the electrophonon coupling term[34] are almost unchanged (see Table S2 for details). NAC is therefore decided by the energy difference term. As shown in the time evolution patterns of the VBM, CBM, and trap states for 1-Ov-LS and 1-Ov-HS in the spin-up channel (Figure 3c,d), the energy difference between Trap 1 and the CBM is 1.61 eV in 1-Ov-HS, whereas it is only 0.81 eV in the 1-Ov-LS. The resulting smaller NAC (Figure S3) restricts path 2 of the hole recombination with electrons on the CBM, greatly improving the hole relaxation time of 1-Ov-HS (Figure 3e).

Figure 4 shows the hole trapping and recombination dynamics information in the spin-down channel. Because of spin symmetry in the electronic structure, the hole recombination dynamics of 1-Ov-LS are identical in the spin-up and down channels. For 1-Ov-HS, however, there are no defect states in the spin-down channel because both defects are in the spin-up channel. Thus, there are two hole recombination pathways for 1-Ov-LS (direct and by-defect recombination) and only one pathway for 1-Ov-HS (direct recombination). As shown in the hole recombination dynamics of 1-Ov-LS (Figure 4a) and 1-Ov-HS (Figure 4b), the e-h recombination is faster by a factor of 8.4 in 1-Ov-LS compared to 1-OV-HS (0.670 and 5.606 ns, respectively). Figure 4c shows the NAC between

https://doi.org/10.1021/acs.nanolett.2c02070
Nano Lett. 2022, 22, 6334−6341

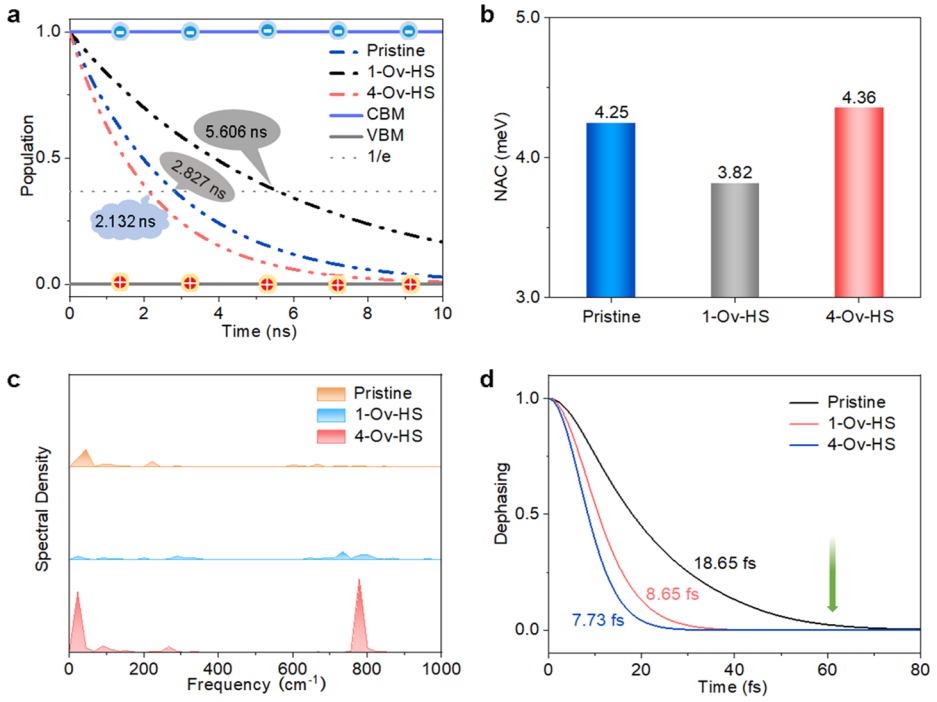

Figure 5. The e-h recombination dynamics between the VBM and the CBM for pristine $BiVO_4$, 1-Ov-LS, and 4-Ov-HS in the spin-down channel. (a) Recombination dynamics. (b) Root-mean-square NAC between the VBM and CBM. (c) Electron−phonon coupling spectra. (d) Pure-dephasing functions.

the key state pairs for 1-Ov-LS and 1-Ov-HS. The NAC involving Trap 1 is absent for 1-Ov-HS because there is no defect state, whereas the NACs between the VBM and the CBM are approximately equal in the two systems. Thus, in comparison to 1-Ov-LS the charge recombination of 1-Ov-HS is greatly improved. Figure 4d shows a schematic of the e-h recombination processes in the spin-down channel for 1-Ov-LS and 1-Ov-HS. The existence of the trap states in 1-Ov-LS means that the carriers easily recombine through the by-defect pathway, but this is not possible for 1-OV-HS. $BiVO_4$ contains heavy elements, in particular Bi, and therefore significant spin−orbit interaction can be expected, leading to spin flips. Spin flips will have no influence on the quantum dynamics in the low spin state, because both channels have the same energy levels, Figure 2c. In the high spin state, the spin-up channel has two midgap states, while the other channel has no midgap states, Figure 2d. By focusing on the channel with the midgap states, we provided the lower bound on the recombination time. Recombination in the other channel without the midgap states is slower. Hence, spin flips caused by spin−orbit coupling will introduce a slower charge recombination component. The charge recombination dynamics of 1-Ov-HS are better than 1-Ov-LS in both the spin-up and down channels. Hence, the total carrier lifetime of 1-Ov-HS is excellent compared to 1-Ov-LS, and we term this way of improving carrier dynamics the SPM.

We hypothesize that the SPM also applies to systems with a higher Ov concentration and therefore we study the e-h recombination dynamics of the spin-polarized system with different Ov concentrations. We focused on the spin-down channel with no trap states to study the SPM with variable Ov concentration; the carrier dynamics of the spin-up channel is complicated by the introduction of multiple recombination pathways with higher Ov concentrations (more information in Figures S7 and S8). The e-h recombination information (Table S3) for the spin-down channel of the pristine, 1-Ov-HS, and 4-Ov-HS $BiVO_4$ systems is shown in Figure 5. The shortest carrier lifetime was observed for the 4-Ov system (2.132 ns) as shown in Figure 5a. The average absolute NAC values of the pristine, 1-Ov-HS, and 4-Ov-HS $BiVO_4$ systems are 4.25, 3.82, and 4.36 meV, respectively, as shown in Figure 5b. Because of minor changes in the reduced masses of the relevant vibrational motions, the nuclear velocity term in eq S1 varies little across the systems at a given temperature. Figure S9 shows the fluctuations of the VBM and CBM in the three $BiVO_4$ systems. The average band gaps are nearly identical, meaning that the band gap is not the crucial factor for variation of the NAC. We note that the average band gap at 300 K is 2.3 eV, compared with 2.4 eV for the optimized geometry at 0 K. This change is caused by the temperature renormalization.[35,36] The standard deviations (S in Figure S9) of the VBM and CBM increase with the Ov concentration, as a result of more broken bonds and more phonon modes contributing to the electron−phonon couplings. As seen from Figure 5c, the dominant phonon modes are low frequency in the pristine system. In comparison, phonon modes around 700−800 cm^{-1} appear with lower intensity in the 1-Ov system, while strong signals in both low (30 cm^{-1}) and high frequency (750 cm^{-1}) regions are present in the 4-Ov system. Both frequencies and intensities in the electron−phonon coupling spectrum increase with the number of broken bonds. Compared with the increase in the phonon frequency and signal intensity, the reduction in the wave function overlap between the VBM and the CBM is insignificant. The pure-dephasing time[37] characterizes elastic electron-vibrational scattering that is responsible for the vibrationally induced loss of coherence within the electronic subsystem. In Figure 5d, the pure-dephasing time of 1-Ov is less than half of that for the pristine system, and only slightly longer than for 4-Ov. The spin charge density confirms that the difference is mainly due to the CBM charge density change

https://doi.org/10.1021/acs.nanolett.2c02070
Nano Lett. 2022, 22, 6334−6341

(Figure S10). The CBM charge density is distributed primarily on the V atoms, while the excess electrons contributed by the oxygen vacancy are localized in the conduction orbitals of several V atoms. However, the charge density of the CBM changes little between the 1-Ov and 4-Ov systems. Consequently, compared with the pristine system the electron−phonon coupling term decreases for 1-Ov and increases for 4-Ov. The data indicate the decreased wave functions overlap does not neutralize the increased number of modes contributing to the electron−phonon coupling term in eq S1. The NAC can be minimized by adjusting the Ov concentration to mediate competition between the number of active phonon modes and the overlap of electron and hole states.

The nonradiative e-h recombination dynamics are governed by the nonadiabatic coupling, composed by the three terms described in eq S1. This provides a theoretical rationale for improving the carrier lifetime in materials. The results show, first, that the high spin-polarized Ov system provides a new SPM strategy for improving the e-h recombination dynamics of solar energy conversion and optoelectronic materials by minimizing the adverse effects of oxygen vacancies. Second, the carrier lifetime of the $BiVO_4$ system can be optimized by adjusting the Ov concentration to mediate competition between the atom thermal motion-assisted electron−phonon coupling and the overlap of electron and hole states to minimize the nonadiabatic coupling. The tendency of the carrier lifetime to vary demonstrates that both balancing the optimum Ov concentration in $BiVO_4$ and minimizing the Ov concentration are viable strategies for increasing the device efficiency. We posit that this strategy can be applied to other materials in which the impact of defects is tied to the spin polarization.[26]

The defect concentration used in the simulations is high due to computational limitations on the size of the simulation cell. Defect concentration is significantly lower in experiments, and large regions of the material are bulklike. The SRH process of defect-mediate recombination puts emphasis on defects because charge trapping by defects is faster than bulklike charge recombination. In our simulations, the charge trapping occurs on 0.01−0.1 ns time scale, according to the rise of the trap state populations (Figure 3a,b), whereas subsequent recombination of the trapped charges takes around 1 ns. In materials with large dielectric constants, ∼86 for $BiVO_4$,[38] electron−hole interactions are screened, and charges are separated and need to diffuse to each other in order to recombine. Defect localizes one charge, and diffusion of only the other charge toward the defect site is required. At low charge concentrations, a free charge can find the trapped charge more easily than another free charge, and defect-mediated recombination is the dominant mechanism, as the SRH statistics indicate.[39]

The influence of defects on nonradiative charge recombination in new classes of semiconductors is more complex than suggested by the classic SRH model, as exemplified by metal halide perovskites,[34] and can be controlled by the spin state, as demonstrated in the present work. Even though defects do not always accelerate carrier recombination, they reduce charge mobility due to enhancement in charge scattering and trapping, undermine chemical stability, and so forth.[16] At the same time, the high chemical reactivity of defect sites forms the basis for photo- and electro-catalysis in which long lifetimes of defect states is particularly beneficial.

To summarize, using time-dependent ab initio NAMD simulations, we have investigated the e-h recombination dynamics of different electronic spin structures and varying concentrations of Ov in bulk $BiVO_4$. Despite the identical concentration of Ov in 1-Ov-LS and 1-Ov-HS, the high spin polarization of the latter leads to superior carrier dynamics with e-h recombination inhibited by the SPM. Moderating the Ov concentration can maximize the SPM effect to suppress the charge recombination by minimizing the electron−phonon coupling arising from atomic thermal motions, and electron−hole overlap. We propose that these conclusions are applicable to other materials with triplet spin vacancies that, similar to $BiVO_4$, can be tuned in by controlling defect concentration and electronic spin structure to reduce nonradiative charge recombination and improve spin character.

■ ASSOCIATED CONTENT

Supporting Information

The Supporting Information is available free of charge at https://pubs.acs.org/doi/10.1021/acs.nanolett.2c02070.

Details of the calculation methods, plots of the relaxation dynamics, pure-dephasing functions and electron-vibrational influence spectra, tables of the nonadiabatic coupling, pure-dephasing times, energy gaps and relaxation times, charge densities and evolutions of the energy levels of the key states, atomistic structures and densities of states, and relative total energies of the systems (PDF)

■ AUTHOR INFORMATION

Corresponding Authors

Maochang Liu − *International Research Center for Renewable Energy, State Key Laboratory of Multiphase Flow, Xi'an Jiaotong University, Xi'an, Shaanxi 710049, P.R. China; Suzhou Academy of Xi'an Jiaotong University, Suzhou, Jiangsu 215123, P.R. China;* orcid.org/0000-0002-2371-4060; Email: maochangliu@mail.xjtu.edu.cn

Oleg V. Prezhdo − *Deparments of Chemistry, Physics, and Astronomy, University of Southern California, Los Angeles, California 90089, United States;* orcid.org/0000-0002-5140-7500; Email: prezhdo@usc.edu

Authors

Chunyang Zhang − *International Research Center for Renewable Energy, State Key Laboratory of Multiphase Flow, Xi'an Jiaotong University, Xi'an, Shaanxi 710049, P.R. China*

Yongliang Shi − *Center for Spintronics and Quantum Systems, State Key Laboratory for Mechanical Behavior of Materials, School of Materials Science and Engineering, Xi'an Jiaotong University, Xi'an, Shaanxi 710049, China*

Yitao Si − *International Research Center for Renewable Energy, State Key Laboratory of Multiphase Flow, Xi'an Jiaotong University, Xi'an, Shaanxi 710049, P.R. China*

Liejin Guo − *International Research Center for Renewable Energy, State Key Laboratory of Multiphase Flow, Xi'an Jiaotong University, Xi'an, Shaanxi 710049, P.R. China;* orcid.org/0000-0001-9412-3260

Jin Zhao − *ICQD/Hefei National Laboratory for Physical Sciences at the Microscale, and CAS Key Laboratory of Strongly-Coupled Quantum Matter Physics, and Department of Physics and Synergetic Innovation Center of Quantum*

https://doi.org/10.1021/acs.nanolett.2c02070
Nano Lett. 2022, 22, 6334−6341

Information and Quantum Physics, University of Science and Technology of China, Hefei, Anhui 230026, China;
orcid.org/0000-0003-1346-5280

Complete contact information is available at:
https://pubs.acs.org/10.1021/acs.nanolett.2c02070

Author Contributions

[▽]C.Z., Y. S., and Y.S. contributed equally.

Notes

The authors declare no competing financial interest.

■ ACKNOWLEDGMENTS

We would like to thank Prof. Wenshuai Chen and Prof. Naixu Li for helpful discussion. We gratefully acknowledge HZWTECH for providing computation facilities. We also gratefully acknowledge the financial support by the National Natural Science Foundation of China (No. 51888103, No. 51876173), the Natural Science Foundation of Jiangsu Province (No. BK20190054), the Suzhou Science and Technology Program (SYG202101), Fok Ying-Tung Education Foundation (No. 171048), the China Fundamental Research Funds for the Central Universities, the National Natural Science Foundation of China (No. 11904353), the Open Project of State Key Laboratory of Surface Physics (No. KF2020_10) Sciences (Ministry of Education), and the U.S. Natural Science Foundation (No. CHE-2154367).

■ REFERENCES

(1) Appavoo, K.; Liu, M. Z.; Black, C. T.; Sfeir, M. Y. Quantifying Bulk and Surface Recombination Processes in Nanostructured Water Splitting Photocatalysts Via in Situ Ultrafast Spectroscopy. *Nano Lett.* **2015**, *15*, 1076−1082.

(2) Zhang, S.; Wang, J.; Wen, S.; Jiang, M.; Xiao, H.; Ding, X.; Wang, N.; Li, M.; Zu, X.; Li, S.; Yam, C.; Huang, B.; Qiao, L. Approaching Charge Separation Efficiency to Unity without Charge Recombination. *Phys. Rev. Lett.* **2021**, *126*, 176401.

(3) Rizzo, D. J.; Jessen, B. S.; Sun, Z. Y.; Ruta, F. L.; Zhang, J.; Yan, J. Q.; Xian, L. D.; McLeod, A. S.; Berkowitz, M. E.; Watanabe, K.; Taniguchi, T.; Nagler, S. E.; Mandrus, D. G.; Rubio, A.; Fogler, M. M.; Millis, A. J.; Hone, J. C.; Dean, C. R.; Basov, D. N. Charge-Transfer Plasmon Polaritons at Graphene/Alpha-$RuCl_3$ Interfaces. *Nano Lett.* **2020**, *20*, 8438−8445.

(4) Neukirch, A. J.; Nie, W. Y.; Blancon, J. C.; Appavoo, K.; Tsai, H.; Sfeir, M. Y.; Katan, C.; Pedesseau, L.; Even, J.; Crochet, J. J.; Gupta, G.; Mohite, A. D.; Tretiak, S. Polaron Stabilization by Cooperative Lattice Distortion and Cation Rotations in Hybrid Perovskite Materials. *Nano Lett.* **2016**, *16*, 3809−3816.

(5) Ball, J. M.; Petrozza, A. Defects in Perovskite-Halides and Their Effects in Solar Cells. *Nat. Energy* **2016**, *1*, 1−13.

(6) Xu, M.; Gao, Y.; Moreno, E. M.; Kunst, M.; Muhler, M.; Wang, Y.; Idriss, H.; Wöll, C. Photocatalytic Activity of Bulk TiO_2 Anatase and Rutile Single Crystals Using Infrared Absorption Spectroscopy. *Phys. Rev. Lett.* **2011**, *106*, 138302.

(7) Yoo, J. J.; Seo, G.; Chua, M. R.; Park, T. G.; Lu, Y.; Rotermund, F.; Kim, Y.-K.; Moon, C. S.; Jeon, N. J.; Correa-Baena, J.-P.; Bulovic, V.; Shin, S. S.; Bawendi, M. G.; Seo, J. Efficient Perovskite Solar Cells Via Improved Carrier Management. *Nature* **2021**, *590*, 587−593.

(8) Svatek, S. A.; Kerfoot, J.; Summerfield, A.; Nizovtsev, A. S.; Korolkov, V. V.; Taniguchi, T.; Watanabe, K.; Antolin, E.; Besley, E.; Beton, P. H. Triplet Excitation and Electroluminescence from a Supramolecular Monolayer Embedded in a Boron Nitride Tunnel Barrier. *Nano Lett.* **2020**, *20*, 278−283.

(9) Zhou, M.; Higaki, T.; Hu, G.; Sfeir, M. Y.; Chen, Y.; Jiang, D.-e.; Jin, R. Three-Orders-of-Magnitude Variation of Carrier Lifetimes with Crystal Phase of Gold Nanoclusters. *Science* **2019**, *364*, 279−282.

(10) Cao, K. C.; Zoberbier, T.; Biskupek, J.; Botos, A.; McSweeney, R. L.; Kurtoglu, A.; Stoppiello, C. T.; Markevich, A. V.; Besley, E.; Chamberlain, T. W.; Kaiser, U.; Khlobystov, A. N. Comparison of Atomic Scale Dynamics for the Middle and Late Transition Metal Nanocatalysts. *Nat. Commun.* **2018**, *9*, 1−10.

(11) Corby, S.; Rao, R. R.; Steier, L.; Durrant, J. R. The Kinetics of Metal Oxide Photoanodes from Charge Generation to Catalysis. *Nat. Rev. Mater.* **2021**, *6*, 1136−1155.

(12) Latini, S.; Ronca, E.; De Giovannini, U.; Hubener, H.; Rubio, A. Cavity Control of Excitons in Two-Dimensional Materials. *Nano Lett.* **2019**, *19*, 3473−3479.

(13) Liu, M.; Jing, D.; Zhou, Z.; Guo, L. Twin-Induced One-Dimensional Homojunctions Yield High Quantum Efficiency for Solar Hydrogen Generation. *Nat. Commun.* **2013**, *4*, 1−8.

(14) Zhao, D.; Wang, Y.; Dong, C.-L.; Huang, Y.-C.; Chen, J.; Xue, F.; Shen, S.; Guo, L. Boron-Doped Nitrogen-Deficient Carbon Nitride-Based Z-Scheme Heterostructures for Photocatalytic Overall Water Splitting. *Nat. Energy* **2021**, *6*, 388−397.

(15) Huang, Y.; Yu, Y.; Yu, Y.; Zhang, B. Oxygen Vacancy Engineering in Photocatalysis. *Sol. RRL* **2020**, *4*, 2000037.

(16) Sandberg, O. J.; Zeiske, S.; Zarrabi, N.; Meredith, P.; Armin, A. Charge Carrier Transport and Generation Via Trap-Mediated Optical Release in Organic Semiconductor Devices. *Phys. Rev. Lett.* **2020**, *124*, 128001.

(17) Yan, D.; Li, Y.; Huo, J.; Chen, R.; Dai, L.; Wang, S. Defect Chemistry of Nonprecious-Metal Electrocatalysts for Oxygen Reactions. *Adv. Mater.* **2017**, *29*, 1606459.

(18) Motti, S. G.; Meggiolaro, D.; Barker, A. J.; Mosconi, E.; Perini, C. A. R.; Ball, J. M.; Gandini, M.; Kim, M.; De Angelis, F.; Petrozza, A. Controlling Competing Photochemical Reactions Stabilizes Perovskite Solar Cells. *Nat. Photonics* **2019**, *13*, 532−539.

(19) Shockley, W.; Read, W., Jr Statistics of the Recombinations of Holes and Electrons. *Phys. Rev.* **1952**, *87*, 835.

(20) Qiu, W.; Xiao, S.; Ke, J.; Wang, Z.; Tang, S.; Zhang, K.; Qian, W.; Huang, Y.; Huang, D.; Tong, Y.; Yang, S. Freeing the Polarons to Facilitate Charge Transport in $BiVO_4$ from Oxygen Vacancies with an Oxidative 2d Precursor. *Angew. Chem., Int. Ed.* **2019**, *131*, 19263−19271.

(21) Wang, S.; Pan, L.; Song, J.-J.; Mi, W.; Zou, J.-J.; Wang, L.; Zhang, X. Titanium-Defected Undoped Anatase TiO_2 with P-Type Conductivity, Room-Temperature Ferromagnetism, and Remarkable Photocatalytic Performance. *J. Am. Chem. Soc.* **2015**, *137*, 2975−2983.

(22) Wu, S.-M.; Liu, X.-L.; Lian, X.-L.; Tian, G.; Janiak, C.; Zhang, Y.-X.; Lu, Y.; Yu, H.-Z.; Hu, J.; Wei, H.; Zhao, H.; Chang, G.-G.; Van Tendeloo, G.; Wang, L.-Y.; Yang, X.-Y.; Su, B.-L. Homojunction of Oxygen and Titanium Vacancies and Its Interfacial N−P Effect. *Adv. Mater.* **2018**, *30*, 1802173.

(23) Pan, L.; Wang, S.; Mi, W.; Song, J.; Zou, J.-J.; Wang, L.; Zhang, X. Undoped Zno Abundant with Metal Vacancies. *Nano Energy* **2014**, *9*, 71−79.

(24) Pan, L.; Ai, M.; Huang, C.; Yin, L.; Liu, X.; Zhang, R.; Wang, S.; Jiang, Z.; Zhang, X.; Zou, J.-J.; Mi, W. Manipulating Spin Polarization of Titanium Dioxide for Efficient Photocatalysis. *Nat. Commun.* **2020**, *11*, 1−9.

(25) Corby, S.; Francas, L.; Kafizas, A.; Durrant, J. R. Determining the Role of Oxygen Vacancies in the Photoelectrocatalytic Performance of WO_3 for Water Oxidation. *Chem. Sci.* **2020**, *11*, 2907−2914.

(26) Wang, S.; He, T.; Chen, P.; Du, A.; Ostrikov, K.; Huang, W.; Wang, L. In Situ Formation of Oxygen Vacancies Achieving Near-Complete Charge Separation in Planar $BiVO_4$ Photoanodes. *Adv. Mater.* **2020**, *32*, 2001385.

(27) Hongzhiwei Technology, Device Studio, Version 2021A, China, 2021; available Online: https://iresearch.net.cn/cloud-software (accessed 18 October, 2021).

(28) Katriel, J.; Pauncz, R. Theoretical Interpretation of Hund's Rule. *Adv. Quant. Chem.* **1977**, *10*, 143−185.

(29) Garcés-Pineda, F. A.; Blasco-Ahicart, M.; Nieto-Castro, D.; López, N.; Galán-Mascarós, J. R. Direct magnetic enhancement of

electrocatalytic water oxidation in alkaline media. *Nat. Energy* **2019**, *4*, 519−525.
(30) Zheng, Q.; Chu, W.; Zhao, C.; Zhang, L.; Guo, H.; Wang, Y.; Jiang, X.; Zhao, J. Ab Initio Nonadiabatic Molecular Dynamics Investigations on the Excited Carriers in Condensed Matter Systems. *Wires. Comput. Mol. Sci.* **2019**, *9*, 1411.
(31) Chu, W.; Saidi, W. A.; Zhao, J.; Prezhdo, O. V. Soft Lattice and Defect Covalency Rationalize Tolerance of B-$CsPbI_3$ Perovskite Solar Cells to Native Defects. *Angew. Chem., Int. Ed.* **2020**, *59*, 6435−6441.
(32) Wu, Y. F.; Chu, W. B.; Vasenko, A. S.; Prezhdo, O. V. Common Defects Accelerate Charge Carrier Recombination in $CsSnI_3$ without Creating Mid-Gap States. *J. Phys. Chem. Lett.* **2021**, *12*, 8699−8705.
(33) Zheng, Q.; Saidi, W. A.; Xie, Y.; Lan, Z.; Prezhdo, O. V.; Petek, H.; Zhao, J. Phonon-Assisted Ultrafast Charge Transfer at Van Der Waals Heterostructure Interface. *Nano Lett.* **2017**, *17*, 6435−6442.
(34) Chu, W.; Zheng, Q.; Prezhdo, O. V.; Zhao, J.; Saidi, W. A. Low-Frequency Lattice Phonons in Halide Perovskites Explain High Defect Tolerance toward Electron-Hole Recombination. *Sci. Adv.* **2020**, *6*, 7453.
(35) Wiktor, J.; Reshetnyak, I.; Ambrosio, F.; Pasquarello, A. Comprehensive Modeling of the Band Gap and Absorption Spectrum of $BiVO_4$. *Phys. Rev. Mater.* **2017**, *1*, 022401.
(36) Giustino, F.; Louie, S. G.; Cohen, M. L. Electron-Phonon Renormalization of the Direct Band Gap of Diamond. *Phys. Rev. Lett.* **2010**, *105*, 265501.
(37) Su, J.; Zheng, Q.; Shi, Y.; Zhao, J. Interlayer Polarization Explains Slow Charge Recombination in Two-Dimensional Halide Perovskites by Nonadiabatic Molecular Dynamics Simulation. *J. Phys. Chem. Lett.* **2020**, *11*, 9032−9037.
(38) Wang, Q.; He, J.; Shi, Y.; Zhang, S.; Niu, T.; She, H.; Bi, Y.; Lei, Z. Synthesis of MFe_2O_4 (M= Ni, Co)/$BiVO_4$ film for photo-lectrochemical hydrogen production activity. *Appl. Catal. B Environ.* **2017**, *214*, 158−167.
(39) Das, B.; Aguilera, I.; Rau, U.; Kirchartz, T. What is a deep defect? Combining Shockley-Read-Hall statistics with multiphonon recombination theory. *Phys. Rev. Mater.* **2020**, *4*, 024602.

https://doi.org/10.1021/acs.nanolett.2c02070
Nano Lett. 2022, 22, 6334−6341